Hindawi
Journal of Nanomaterials
Volume 2018, Article ID 9592610, 12 pages
https://doi.org/10.1155/2018/9592610

Research Article

Pressure Sensitive Sensors Based on Carbon Nanotubes, Graphene, and Its Composites

Asar Ali,[1] **Adam Khan**,[2] **Kh. S. Karimov**,[3] **Amjad Ali**,[1] **and Adnan Daud Khan**[1]

[1]*Department of Electrical Engineering, Sarhad University of Science & Information Technology, Peshawar, Pakistan*
[2]*Department of Electronic Engineering, University of Engineering & Technology Peshawar, Abbottabad Campus, Peshawar, Pakistan*
[3]*Faculty of Electronic Engineering, GIK Institute of Engineering Sciences and Technology, Topi, Pakistan*

Correspondence should be addressed to Asar Ali; engrasar45@gmail.com

Received 7 June 2017; Revised 20 July 2017; Accepted 4 January 2018; Published 31 January 2018

Academic Editor: Stefano Bellucci

Carbon nanotubes (CNTs) and graphene have attracted a great deal of interest due to their outstanding mechanical, optical, electrical, and structural properties. Most of the scientists and researchers have investigated the optical and electrical properties of these materials. However, due to unique electromechanical properties of these materials, it is required to explore the piezoresistive properties of bulk nanostructured CNTs, graphene, and CNT-graphene composites. We investigated and compared the sensitivities and piezoresistive properties of sandwich-type pure CNT, pure graphene, and CNT-graphene composite pressure sensors. For all the samples, increase in pressure from 0 to 0.183 kNm^{-2} results in a decrease in the impedance and direct current (DC) resistance. Sensitivity and percentage decrease in resistance and impedance of CNT-graphene composite were lower than pure CNT while being higher than pure graphene based sample. Moreover, under the same external applied pressure, the sensitivity and percentage decrease in impedance for pure CNT, pure graphene, and CNT-graphene composite were smaller than the corresponding sensitivity and percentage decrease in resistance. The achieved experimental results of the composite sample were compared with simulated results which exhibit reasonable agreement with each other. The deviations of simulated resistance-pressure and impedance-pressure curves from experimental graphs were 0.029% and 0.105%, respectively.

1. Introduction

The concept of nanomaterials was presented by Herbert Gleiter for the first time over 20 years back. Since then, research interest in the field of nanostructured materials has grown rapidly. The unusual properties, potential applications, and scientific and technological importance of these materials lead them to the current advancement in the sensing technology [1, 2]. Carbon nanotubes (CNTs) and graphene are the two most important representatives of the nanostructural materials [3]. Its density is six times lower than steel. The tensile strength and elasticity of carbon nanotubes (CNTs) are hundred and five times higher than steel, respectively [4]. On the other hand, graphene can withstand with a strain up to 20% and its Young's modulus is almost six hundred and thousand times higher than semiconductors and metals, respectively [5, 6].

These unique electromechanical properties have made CNTs and graphene the most suitable materials for pressure sensing technology. Therefore, CNTs and graphene have been employed in various electronic devices such as pressure sensors, gas sensor, displacement sensors, strain sensors, temperature sensors, humidity sensors, solar cells, and chemical sensors [7–9]. Pressure sensor is one of the promising sensing elements in the sensing technology. Pressure sensing elements can be used in touch screen devices, automotive industry, aviation, biomedical measurements, and so forth. [10]. Most of the pressure sensors are fabricated on the base of inductive, capacitive, and piezoresistive phenomena that can be employed to control and monitor the pressure in various practical applications [11]. Capacitive pressure sensors show somewhat nonlinear behavior to the input stimuli. Inductive pressure sensors are required complex fabrication techniques because it is difficult to bring the materials into coil shape.

Also, leakage of the induced e.m.f. and magnetic flux in the inductive pressure sensors can affect the neighborhood circuitry. Hence, it is difficult to get an accurate response of the inductive pressure sensors. Piezoresistive pressure sensors exhibit outstanding promise for real time applications because of its easy fabrication process, easy signal collection, low cost, and simple device structure [12]. Therefore, a large number of CNTs, graphene, and its composite-based piezoresistive sensing elements have been investigated. Li et al. [13] enhanced the mechanical and piezoresistive properties of graphene by preparing graphene/CNTs hybrid foam (GCFs) by facile self-assembly process. Sahatiya and Badhulika [14] patterned MWCNTs on pencil eraser to develop skin like strain and pressure sensor. The sensitivity and gauge factor of the sensor were 0.135 Mpa^{-1} and 2.4, respectively. Yao et al. demonstrated a high sensitive flexible piezoresistive pressure sensor based on micropatterned films with the layer of carbon nanotubes. The fabricated sensor was applied to measure the pressure of fluid in a curved shaped microtube [15]. Flexible resistive tensile MWCNTs/rubber load sensors were fabricated and investigated by Karimov et al. As the force was increased up to 0.045 N, a 1.37-time average increase in the resistance of the sensors was observed [16]. Khan et al. [17] fabricated and characterized a CNT-VO_2 (3fl) composite piezoresistive pressure sensor. A decrease in the sensor resistance with increase in external uniaxial pressure up to 50 kNm^{-2} was observed. Karimov et al. [10] reported CNT-Cu_2O composite-based piezoresistive pressure sensor, and a 3.3-fold decrement in DC resistance of the sensor was noted as the pressure increased up to 37 kNm^{-2}. Xue and Cui [18] fabricated SWNT thin-film transistors on plastic substrates and reported that, with increase in bending of the elastic substrate, the decrement in the resistance of the SWNT thin film was 10 times greater than silicon. Grow et al. [19] investigated piezoresistance of CNTs on deformable thin-film silicon nitride membranes. The maximum gauge factor ($\Delta R/R_\varepsilon$) in silicon was 200, while for SGS and semiconducting tubes it was 850 and 400, respectively. Similarly, a large number of graphene-based pressure sensors have been fabricated and investigated [12, 20–30].

To the best of our knowledge, no sandwich-type piezoresistive pressure sensor based on bulk nanostructured CNT, graphene, and CNT-graphene composite is reported to date. CNT-graphene composites may take the benefits of outstanding features of both the CNTs and graphene, such as low weight, high strength, large flexibility, high fracture toughness, and especially high gauge factor that may have a good impact in the field of pressure sensing technology. From practical point of view, it will be useful to investigate the resistance-pressure relationships to deepen the knowledge about the physical, electrical, and electromechanical properties of the CNTs, graphene, and its composites.

In this work, instead of focusing on the internal complex structures of CNT and graphene, we explored a novel approach to fabricate sandwich-type pure CNT, pure graphene, and CNTs-graphene composite-based piezoresistive pressure sensors. The term "sandwich-type" is used in the sense that both sides of samples were painted with silver paste (Ag/CNT/Ag, Ag/graphene/Ag, Ag/CNT-graphene/Ag) to provide low resistance electrical contacts. The sensitivities and piezoresistive properties of these sensors were investigated and compared. We believe that this approach will further enhance the practical applications of CNTs, graphene, and its composites in the field of nanomaterial based pressure sensors and other electronic devices.

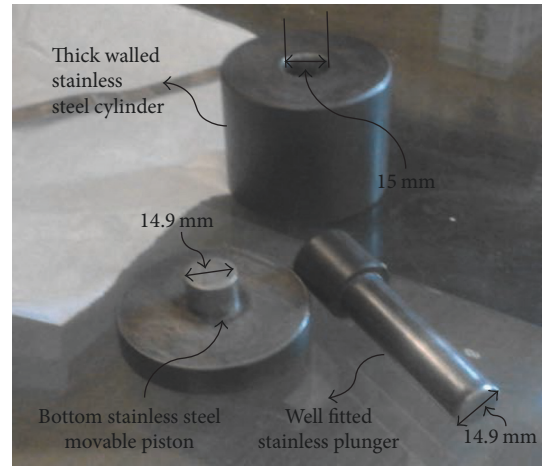

Figure 1: Thick walled stainless steel cylinder, plunger, and piston.

2. Materials and Experimental Details

2.1. Materials. Graphene and multiwalled carbon nanotubes (MWCNTs) powders were commercially purchased from Sun nanotech Co, Ltd. China. According to the supplier, thickness range and area size of the graphene are 5–20 nm and 10 × 10 μm, respectively. The length and diameter range of multiwalled carbon nanotubes (MWCNTs) are 1–10 μm and 10–35 nm, respectively. The purity of MWCNTs is higher than 90%. No further purification was done in the materials. These materials were used for the sample's fabrication as received.

2.2. Sample Preparation. Electronic analytical balance (model: ALS 220-4, weighing range (max): 220 g, readability (d): 0.1 mg, reproducibility: 0.2 mg, linearity: ±0.2 mg) was used to measure the material amount. Initially, the balance was set to zero by pressing the TARE key and then the materials were weighed accurately. CNT (50 wt.%) and graphene (50 wt.%) powder were blended very carefully by utilizing mortar and pestle to make the composite.

A thick walled stainless steel cylinder, stainless steel movable piston, and well fitted stainless steel plunger were utilized to make the samples. The inner diameter of the cylinder was 15 mm, while the outer diameter of each of the movable piston and plunger was 14.9 mm as shown in Figure 1. The bottom of the cylinder was closed by stainless steel movable piston. The blend of the materials was poured into the cylinder from the top. The top of the thick walled stainless steel cylinder was closed by a plunger that was allowed to move down in the cylinder.

To make a durable sample, the material composite within the cylinder was pressed at a pressure of 353 MPa by using hydraulic press. The pellet with diameter of 15 mm and

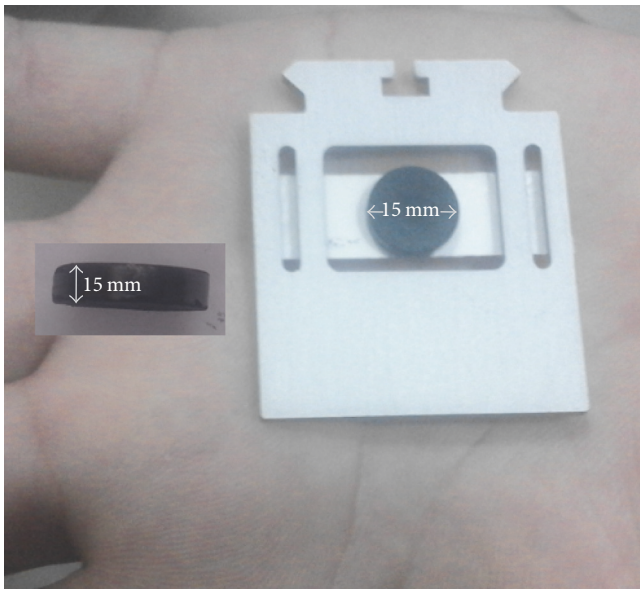

Figure 2: Pressed tablet with 1.5 mm thickness and 15 mm diameter.

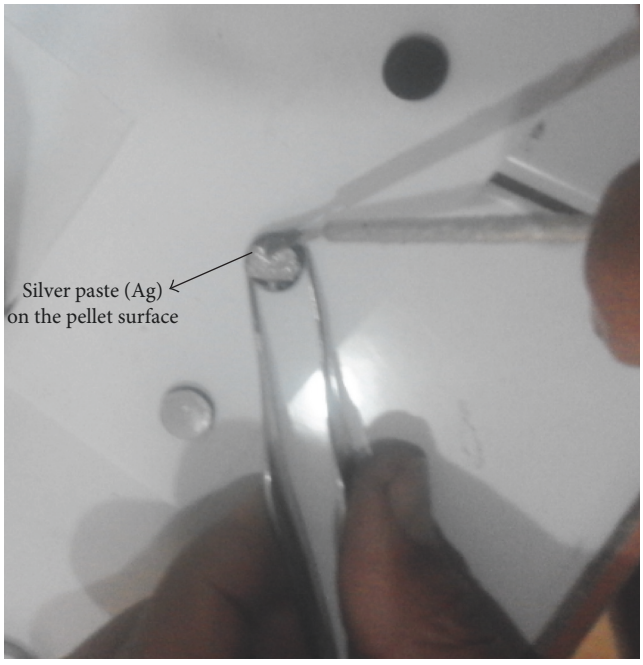

Figure 3: Silver paste (Ag) on both sides of the pressed tablets.

thickness of 1.5 mm was then ejected from the cylinder as shown in Figure 2.

2.3. Measurements and Setup. To provide low resistance electric contacts, both sides of the pressed tablets were covered by silver paste as shown in Figure 3.

Schematic diagram of Ag/sample/Ag, placed on aluminum support with external uniaxial applied pressure is shown in Figure 4. Silver paste (Ag) is assumed as a part of the pellet and has not been shown in the Figure 4. The aluminum

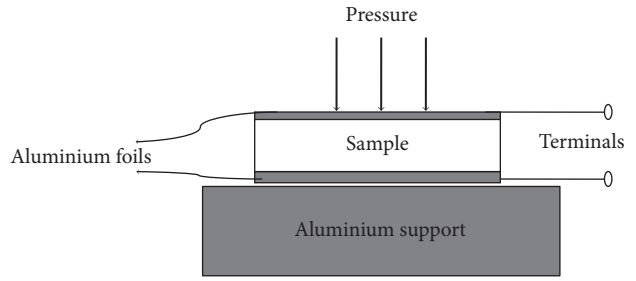

Figure 4: Pressure sensitive element on Al substrate with external applied pressure.

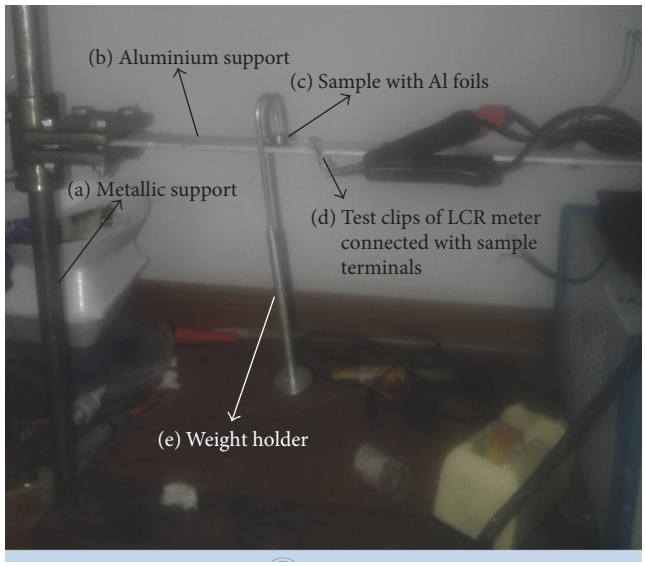

Figure 5: Piezoresistive pressure sample with Al foils installed in experimental setup.

foils are used to act as leads and to avoid scratches on the sample as well.

Figure 5 shows the installment of the sample in experimental setup to investigate its piezoresistive properties. The experimental setup contained the metallic support (a), aluminum support (b), pressure sensitive sensor (pure CNT, pure graphene, and CNT-graphene composite (c)), terminals (d), weight holder (e), and weight (f).

The corresponding conceptual schematic of experimental setup (Figure 5) is depicted in Figure 6. It can be seen from Figure 6 that the piezoresistive pressure element has been placed on aluminum support. The terminals (Al foils) of the sample were connected with the test clips of the MT 4090 LCR Meter. The change in DC resistance of the sensor was noted from the display readings of the MT 4090 LCR Meter. The basic accuracy, ultimate resolution, and measurement range of MT 4090 LCR Meter were 0.2%, 0.001 Ω, and 0.0 Ω to 500 MΩ, respectively.

The pressure value was changed by variation in the weights holding by the weight holder. Weight and weight holder are the major elements of the experimental setup

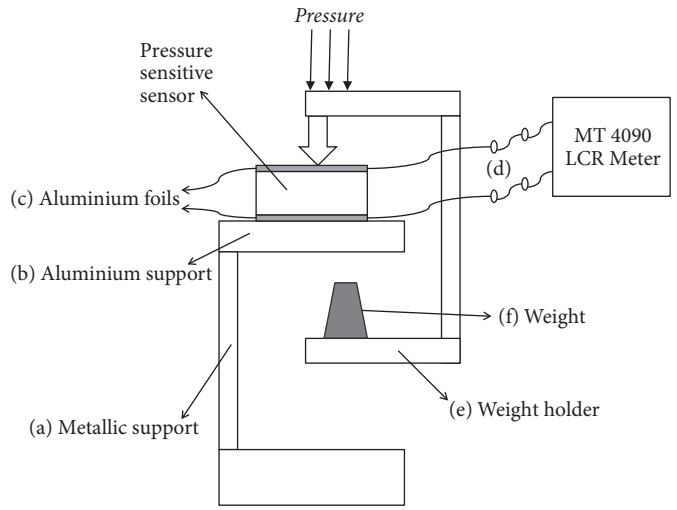

Figure 6: The conceptual schematic view of experimental setup of Figure 5.

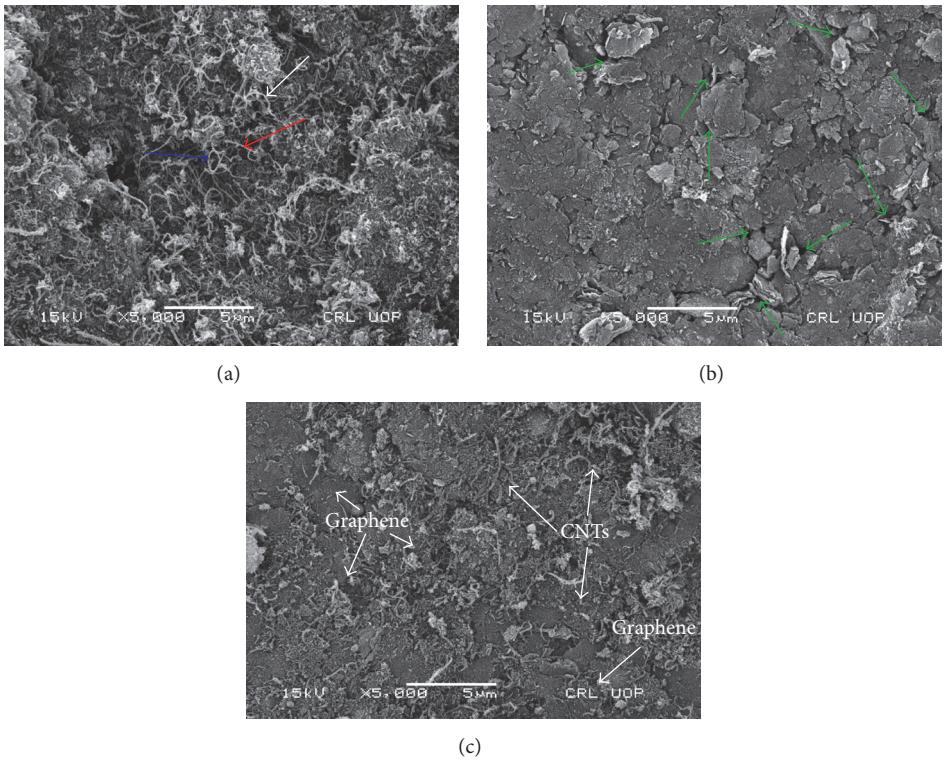

Figure 7: SEM images of (a) pure CNT-based sample, (b) pure graphene-based sample, and (c) CNT-graphene composite-based sample.

utilized from the typical Cantilever Flexure Frame (Flexor) laboratory setup.

3. Results and Discussion

3.1. Scanning Electron Microscopy. The surface morphology of pure CNT, pure graphene, and CNT-graphene composite-based pellets was examined by scanning electron microscope (SEM, model: JSM 5910, energy: 30 kV, magnification (max): 300,000x, resolution power (max): 2.3 nm, manufacturer: JEOL, Japan). The SEM images of pure CNT, pure graphene, and CNT-graphene composite-based pellets are shown in Figure 7. The scale bar is 5 μm in all images (Figures 7(a)–7(c)). As seen in Figure 7(a), the surface morphology of pure CNT-based sample is not uniform. The CNTs are randomly aligned on the surface of the sample. Some of the CNTs seem to be straight (red arrow) and curved in shape (white arrow), but most of them are even circular in shape (blue arrow), which shows that the carbon nanotubes are flexible in nature. The flexibility of CNTs makes them suitable materials for

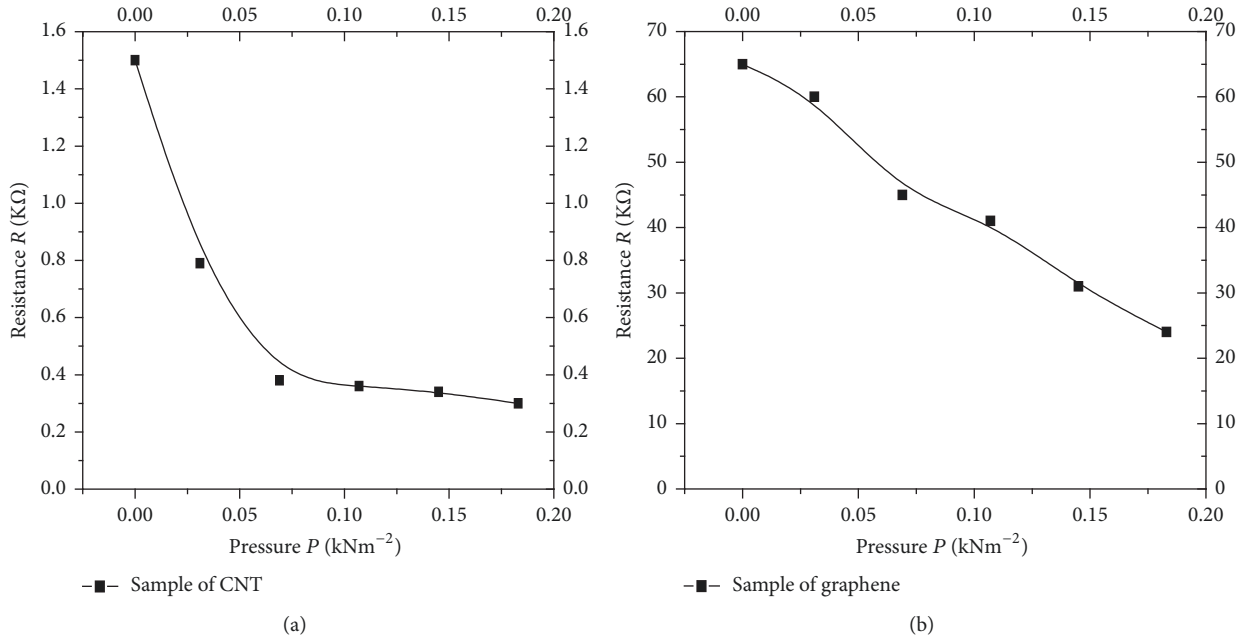

Figure 8: Resistance-pressure relationships of (a) pure CNT and (b) pure graphene-based pressure sensors.

sensing technology. Figure 7(b) reveals that the rough surface of pure graphene-based sample contains higher porosity and dislocations (green arrows) as compared to the pure CNT-based sample (Figure 7(a)). The higher porosity and dislocations in graphene-based sample cause a higher resistance and hence smaller conductivity than pure CNT-based sample (see Section 3.2). Furthermore, graphene nanosheets seem to be densified under the external applied pressure. It can be seen from Figure 7(b) that most of the graphene nanosheets are aligned parallel to each other, which increases the capacitive effect in the sample. The higher capacitance effect leads to smaller impedance (Z) of the graphene sample. Therefore, the impedance (Z) of graphene-based sample is lower than the other two samples (see Sections 3.3 and 3.4).

It can be observed from Figure 7(c) that CNTs and graphene are not uniformly distributed throughout the composite. Multiple contacts between CNTs and graphene particles can be seen in Figure 7(c). The dimensions of graphene nanoparticles seem to be larger than the dimensions of CNTs nanoparticles. The smaller particle size of CNTs reduces the amount of porosity and dislocations which make the CNT-graphene composite sample more uniform as compared to the pure graphene-based sensor (see Section 3.2).

3.2. Resistance-Pressure Relationships. The resistance-pressure relationships for pure CNT and pure graphene-based pressure sensors are shown in Figure 8. It can be seen from Figure 8 that as the external uniaxial pressure increases from 0 kNm^{-2} to 0.183 kNm^{-2}, the DC resistances of the pure CNT (Figure 8(a)) and pure graphene (Figure 8(b)) pressure sensors decrease from 1.5 kΩ to 0.3 kΩ and from 65 kΩ to 24 kΩ, respectively. This shows 80% and 63.24% decrease in DC resistance for CNT and graphene-based samples, respectively. Thickness of the fabricated sample is a significant factor which affects the overall performance of the sample and has an impact on the resistivity and conductivity of the composite materials [31]. Therefore, it is very important to point out the sample thickness dependence on the external applied pressure. Smaller pressure required to compress and deform the thinner sample and vice versa [32]. Even under a smaller external applied pressure, large increase in charge carrier's concentration may completely fill the localized energy states present between the HOMO-LUMO levels which may lead to larger electrical conductivity and hence smaller resistance of the samples [33]. Furthermore, the external uniaxial applied pressure can be equally transferred to every place throughout the thinner samples. Therefore, under the same external applied pressure, this effect increases the mean coordination number, which leads to a more decrease in the resistance of the thinner sample than the thicker one [34].

Resistance-pressure relationship for the CNT-graphene composite-based pressure sensor is shown in Figure 9. It can be observed from Figure 9 that the DC resistance of the CNT-graphene composite-based pressure sensor decreases by 70.32% as the pressure increases from 0 to 0.183 kNm^{-2}. The decrease in resistivity and hence increase in conductivity in the observed resistance-pressure relationship are most probably due to squeezing and densification of CNTs and graphene nanopowder particles under the pressure effect [10]. The decrease percentage in resistance can be computed by the following equation [35]:

$$\%\ \text{decrease in resistance} = \frac{R_o - R}{R_o} * 100, \quad (1)$$

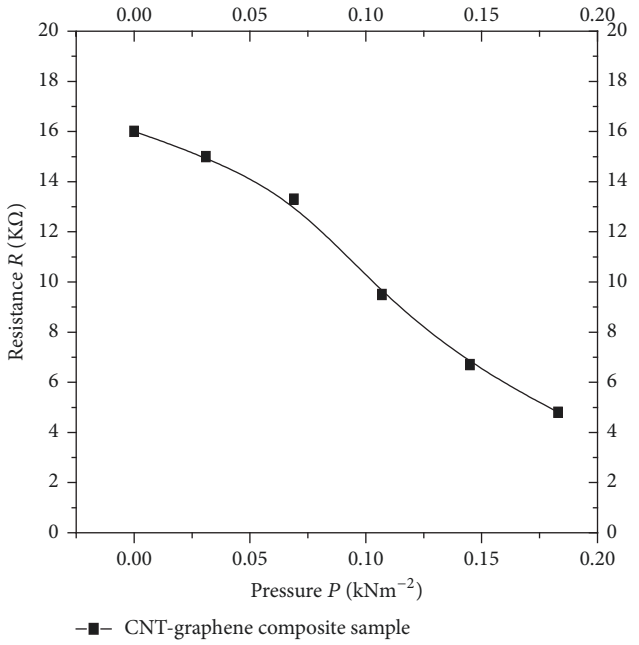

Figure 9: Resistance-pressure relationship for CNT-graphene composite-based pressure sensor.

where R_o is the initial resistance at 0 kNm^{-2} and R is the resistance of the sample at maximum pressure (0.183 kNm^{-2}).

The sensor's resistance (R) can be calculated as [10]

$$R = \frac{d\rho}{A} = \frac{d}{\sigma A}, \tag{2}$$

where d is the interelectrode distance or thickness of the pressed pellet, A is the cross-sectional of pellet, and ρ is the resistivity ($\rho = 1/\sigma$, σ is the conductivity) of the pellet. The total changes in the resistivity of the material due to both the fractional change in resistivity ($\Delta\rho/\rho\varepsilon$) and geometric effects ($1 + 2\upsilon$) can be expressed as [36]

$$\frac{\Delta R}{R_o \varepsilon} = (1 + 2\upsilon) + \frac{\Delta\rho}{\rho\varepsilon},$$
$$\frac{\Delta R}{R_o} = (1 + 2\upsilon)\,\varepsilon + \frac{\Delta\rho}{\rho}. \tag{3}$$

In nanomaterials, the change in resistivity is large enough as compared to the geometrical parameters; hence the geometrical factor is often negligible and the change in the resistivity is dominated in this case [7].

The conductivity mechanism in pure CNT, pure graphene, and CNT-graphene composite-based pressure sensors (2) can be assumed as hopping charge transport between specially separated sites in which charges hop out from one localized state to another to contribute to conductivity [10, 17]. The charge transport mechanism in this random geometry can be described by percolation theory. Percolation theory is widely used in bulk heterojunction systems, conductive polymers, and the composites of nanomaterials because the charge transport mechanism in these materials is based on hopping phenomena [37].

According to the percolation theory, the average conductivity (σ) of pure CNT, pure graphene, and CNT-graphene composite can be calculated using the following expression [7, 38]:

$$\sigma = \frac{1}{LZ}, \tag{4}$$

where L is the characteristic length and depends on the concentration of the localized states and Z is path resistance between sites with the lower average resistance. When external uniaxial pressure increases, the pellets are squeezed between the Al foils (Figures 4–6). This causes a decrease in L and Z, which, in turn, increases the conductivity and hence decreases the resistance of the sensors. This can also be explained as the conduction in disordered nanomaterials limited by the trap states of high potential barrier which exists below the localized states. The trap effect is minimized by filling the trap regions due to increase in the charge carrier's concentration under the squeezing effect that causes an increase in the conductivity and hence decrease in the resistance of the sample [17].

Change in resistance of the sample affects the sensitivity of the sample as well. Large percentage change in resistance increases the sensitivity of the sample.

The sensitivity (S) of all the samples can be calculated as [39]

$$\text{sensitivity } (S) = \frac{\Delta R/R_o}{\Delta P}, \tag{5}$$

where ΔP shows the change in the external uniaxial pressure, R_o denotes the initial resistance at pressure 0 kNm^{-2}, and ΔR is the variation in the DC resistance. The sensitivities of pure CNT (Figure 8(a)), pure graphene (Figure 8(b)), and CNT-graphene composite (Figure 9) samples were 4.37, 3.44, and 3.82 m^2/kN, respectively.

Sensitivity and decrease percentage in the DC resistance for pure CNT, pure graphene, and CNT-graphene composite-based pressure sensors are reported in Table 1. It can be seen from Table 1 that under the same external applied pressure, the decrease percentage in resistance (R) and sensitivity (S) for the pure graphene-based pressure sensor is lower than the other two samples. This can be attributed to two factors: (1) higher structural strength and (2) large particle size. The structural strength of graphene is higher than carbon nanotubes [40].

Under the same external applied pressure, higher structural strength causes smaller deformation in pure graphene sample than the other two samples. This smaller deformation in pure graphene sample leads to a smaller effect on the HOMO-LUMO band-gap of the material, which, in turn, leads to a smaller decrease in the resistance of the sample. Large particle size causes a lower surface area-to-volume ratio, which, in turn, decreases the reactivity of a material to external stimuli [2]. Moreover, large particles sizes of material decrease uniformity and increase dislocations, porosity, and other defects in the material [1]. Most of the carbon nanotubes currently available in the open literature have smaller surface area (100–850 m^{2}g^{-1}) than graphene surface area (up

Table 1: Sensitivity and percentage of decrease in DC resistance for pure CNT, pure graphene, and CNT-graphene composite sensor.

Sensor type	External applied pressure (kNm^{-2})	Percentage decrease in resistance R (%)	Sensitivity (S) (m^2/kN)
Pure CNT	0 to 0.183	80	4.37
Pure graphene	0 to 0.183	63.24	3.44
CNT-graphene composite	0 to 0.183	70.32	3.82

to 2675 m^2g^{-1}) [41, 42]. The large size of graphene nanosheets results in a greater amount of dislocations, porosity, and other defects as compared to carbon nanotubes [1]. Most of the external applied pressure can be absorbed by the dislocations, porosity, and other defects in graphene nanopowder. Therefore, the sensitivity (S) and decrease percentage in resistance R of pure graphene-based pressure sensor are lower than the pure CNT-based sample (Table 1). In case of CNT-graphene composite pressure sensor, it can be assumed that CNTs make the composite more responsive to the external stimuli (pressure in our case) by increasing the uniformity. Therefore, sensitivity and decrease percentage in resistance R of the CNT-graphene composite sample are higher than pure graphene but smaller than pure CNT-based sample. The incorporation of CNTs into graphene increases the uniformity and decreases dislocations, porosity, and other defects in graphene nanopowder, which, in turn, decreases the resistance and hence increases the conductivity of the material. Therefore, CNTs can be considered as an excellent filler to reduce the resistivity and enhance the conductivity of graphene nanopowder.

3.2.1. Relative Resistance-Pressure Relationship. The relative resistance-pressure relationships for pure CNT, pure graphene, and CNT-graphene composite are shown in Figure 10.

The characteristic curves of pure CNT, pure graphene, and their composite (Figure 10) significantly differ from each other due to their very different aspect ratio. The sensors show a significant decrease in DC resistance as the pressure increases from 0 to 0.183 kNm^{-2}; however, the effect is more pronounced in pure CNT-based sensor than the other two. It can be observed from Figure 10 that the pure CNT-based pressure sensor has aggressive slope when the pressure increases from 0 to 0.069 kNm^{-2}. At a pressure level of 0.069 kNm^{-2}, CNT-based pressure sensor reaches its operating limit (saturation) and is almost no longer responsive even when the input stimulus (pressure) is increased beyond this level. Resistance-pressure relationship curve (Figure 10) for pure graphene-based pressure sensor is more uniform than pure CNT-based sensor. Surprisingly, CNT-graphene composite-based pressure sensor shows less aggressive slope to the external uniaxial applied pressure than the other two sensors. The composite-based pressure sensor relative resistance-pressure characteristic exhibits quasi-linear behavior (Figure 10) that can be linearized by using nonlinear operational-amplifiers for practical applications of the sensors [43].

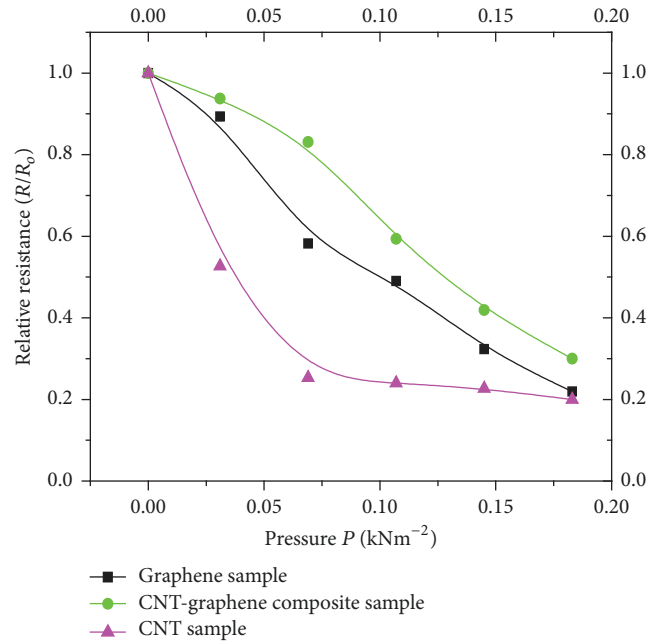

Figure 10: Relative resistance-pressure relationships for pure CNT, pure graphene, and CNT-graphene composite-based pressure sensors.

3.2.2. Experimental versus Simulation. A mathematical formula, which forms a basis for operation of the sensor, can be used to compute the transfer function of the sensor. However, if a solvable formula for the transfer function of a complex sensor does not exist, then one can apply a number of approximations for the transfer function of the sensor. The purpose of the approximation is to fit the observed experimental data with the calculated values of the approximation function. The most important approximations used for the transfer function of the sensors are linear, exponential, and polynomial regression approximation [44]. If none of the linear and exponential approximations are fitting the experimental data well. Then the suitable approximation is polynomial regression model. Unfortunately, this model does not provide enough information about the internal structure and properties of the materials. However, it provides a best fit to the experimental data (Figure 9). If higher accuracy is required, then higher order polynomials can be considered [44]. However, in our case, 3rd order polynomial regression model (6) gives acceptable range of accuracy and a best fit to the experimental data (Figure 9) as shown in Figure 11.

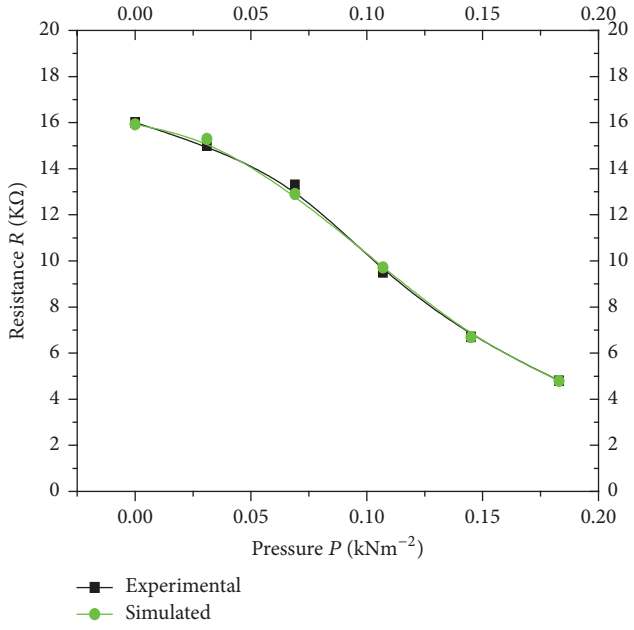

Figure 11: Resistance-pressure relationship of experimental (Figure 9) and simulation (7) for CNT-graphene composite sample.

The selected approximation function (6) is then transferred to the relative values (7). The fitting parameters K_1, K_2, and K_3 (pressure factors) are used to calculate the resistance at various pressure levels. The mathematical model used in the simulation is a polynomial regression model that can be expressed as follows [44]:

$$F(x) = A + K_1 x + K_2 x^2 + K_3 x^3. \quad (6)$$

In our case, (6) can be written in the following form:

$$\frac{R}{R_o} = A + K_1 P + K_2 P^2 + K_3 P^3, \quad (7)$$

where P is the pressure, K_1, K_2, and K_3 are the fitting parameters or pressure factors, A is the intercept, and R_o and R are the resistances of the pellets at initial state and under pressure. The values of A, K_1, K_2, and K_3 calculated at pressure level of 0.183 kNm^{-2} are 15.90686, 5.93051, −922.99399, and 3052.92373 kN^{-2}m^2, respectively.

Experimental data (Figure 9) and simulated results (7) have excellent agreement with each other as shown in Figure 11. The simulated resistance-pressure curve deviates by only 0.029% from the experimental resistance-pressure graph. The deviation of experimental data from simulation can be calculated as [45]

$$\% \text{ deviation} = \frac{\text{Theoritical data} - \text{Experimental data}}{\text{Theoritical data}} * 100. \quad (8)$$

3.3. Impedance-Pressure Relationships. Impedance-pressure relationships for pure CNT and pure graphene-based pressure sensors at 1 kHz are shown in Figure 12.

It can be observed from Figure 12 that as the pressure increases from 0 to 0.183 kNm^{-2}, the impedance of pure CNT (Figure 12(a)) and that of pure graphene (Figure 12(b)) pressure sensors decrease by 72.85% and 48.33%, respectively. The impedance Z of the sample is assumed as parallel connected resistor and capacitor. The equivalent circuit diagram shown in Figure 13 seems to be valid for the sample.

The charge carrier transport occurs through the nanoparticles (resistors) and micropores (capacitors). The impedance (Z) of the equivalent RC circuit of the sample can be calculated using the following equation [46, 47]:

$$Z = \frac{1}{\left[\left(1/R^2\right) + \left(2\pi f C\right)^2\right]^{1/2}} = \frac{1}{Y}, \quad (9)$$

where f is the frequency, Y is the admittance, and R and C represents the resistance and capacitance of the sample, respectively. The capacitance-pressure relationship [11] shows increase in capacitance with increase in pressure. However, in our case, it can be seen that both the resistance and impedance decrease with increase in pressure. The variation in impedance occurs in the same fashion as the variation in the resistance of the sensor. Therefore, it can be concluded that the impedance is more dominated by the resistance effect than the corresponding capacitance effect.

The impedance-pressure relationship for CNT-graphene composite-based pressure sensor at 1 kHz is shown in Figure 14.

The impedance of the composite sample decreases by 64.23% with increase in external uniaxial pressure from 0 to 0.183 kNm^{-2}.

For sensitivity computation, the term $\Delta R/R_o$ in (5) was replaced with $\Delta Z/Z_o$ [39]:

$$\text{sensitivity } (S) = \frac{\Delta Z/Z_o}{\Delta P}. \quad (10)$$

The sensitivities of the pure CNT, pure graphene, and CNT-graphene composite samples were 3.98, 2.64, and 3.53 m^2/kN, respectively. For the same pressure range, decrease percentage in the impedance and corresponding sensitivities for pure CNT, pure graphene, and CNT-graphene composite-based pressure sensors are reported in Table 2. It can be seen from Table 2 that the sensitivity (S) and decrease percentage in impedance Z of the samples is greater in the following order: pure CNT > CNT-graphene composite > pure graphene.

3.3.1. Relative Impedance-Pressure Relationship. The relative impedance-pressure relationships for the three pellets are shown in Figure 15, where the values are measured at a frequency of 1 kHz at room temperature.

The behavior of relative impedance-pressure characteristics shown in Figure 15 is similar to that of relative resistance-pressure characteristics (Figure 10). Therefore, it can be concluded that impedance is more dominated by the resistance effect than the corresponding capacitance effect.

3.3.2. Experimental versus Simulation. The variation in impedance (Figure 14) occurs in the same fashion as the

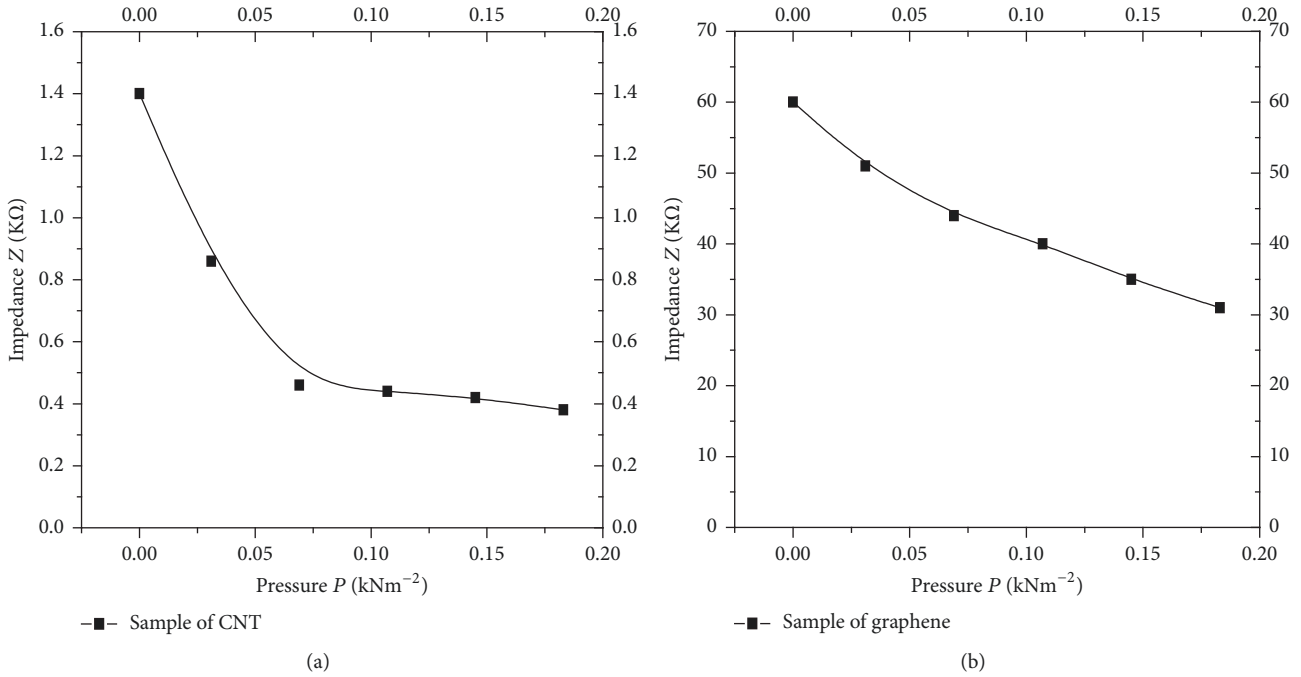

Figure 12: Impedance-pressure relationships of (a) pure CNT and (b) pure graphene-based pressure sensors at 1 KHz.

Table 2: Sensitivity and percentage of decrease in the impedance for pure CNT, pure graphene, and CNT-graphene composite sensors.

Sensor type	External applied pressure (kNm^{-2})	Percentage decrease in impedance Z (%)	Sensitivity (S) (m^2/kN)
Pure CNT	0 to 0.183	72.85	3.98
Pure graphene	0 to 0.183	48.33	2.64
CNT-graphene composite	0 to 0.183	64.23	3.53

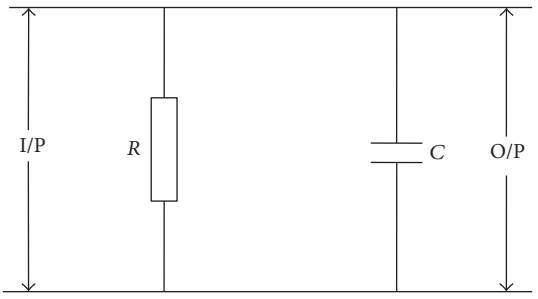

Figure 13: Equivalent RC circuit diagram for the fabricated sample.

variation in resistance (Figure 9) of the sensor. Therefore, for the CNT-graphene composite, R/R_o in (7) can be replaced by Z/Z_o [44]:

$$\frac{Z}{Z_o} = A + K_1P + K_2P^2 + K_3P^3. \quad (11)$$

The values of A, K_1, K_2, and K_3 calculated at pressure level of 0.183 kNm^{-2} are 14.87078, 29.0523, −1097.2955, and 3564.15746 $kN^{-2}m^2$, respectively.

Experimental data (Figure 14) and simulated results (11) have excellent agreement with each other as shown in Figure 16.

The maximum deviation of simulated impedance-pressure graph from experimental curve is 0.105% only.

3.4. Resistance versus Impedance. The decrease percentage values in impedance (Table 2) for pure CNT, pure graphene, and CNT-graphene composite are smaller than the corresponding values of decrease percentage in resistance (Table 1). This is due to the additional resistance offered by the reactance ($2\pi fc$) in the denominator of (9). Under the same external applied pressure, the decrease percentages in Z (Table 2) for pure CNT, pure graphene, and CNT-graphene composite are, respectively, 8.9%, 24.57%, and 8.66% smaller than the corresponding decrease percentages in resistances (Table 1). For graphene sample, the higher reduction in Z (24.57%) is due to the fact that the impedance Z of the sample is inversely proportional to the capacitance of the sample (9); that is, the value of Z decreases with the increase in C. Also, large plate area causes more charge collection that results in greater capacitance of the capacitor. The surface area of graphene nanosheets (2675 m^2g^{-1}) is larger than the surface area of

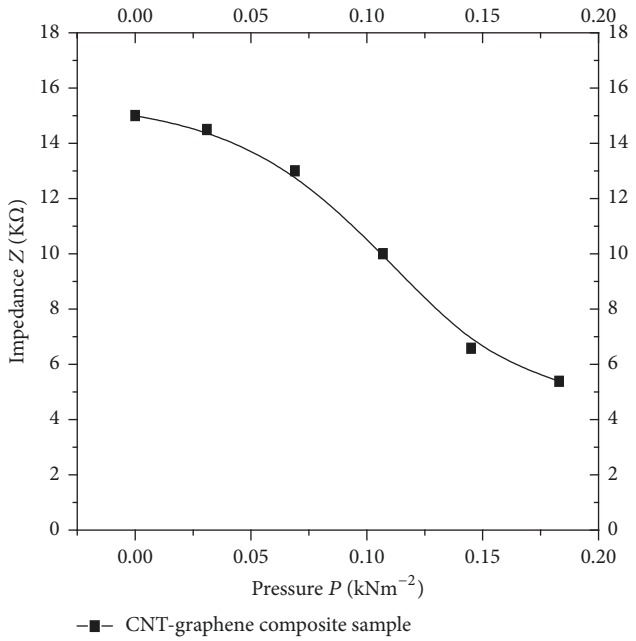

Figure 14: Impedance-pressure relationship for CNT-graphene composite-based pressure sensor at 1 kHz.

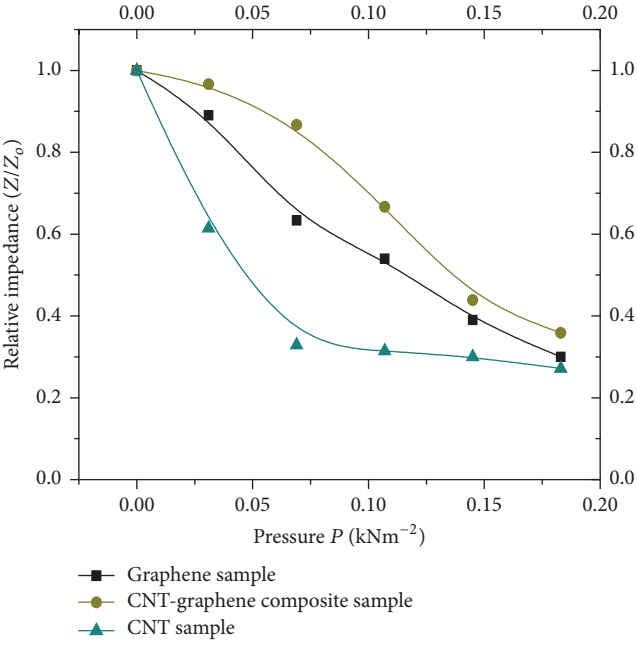

Figure 15: Relative impedance-pressure relationships for pure CNT, pure graphene, and CNT-graphene composite-based pressure sensor at 1 kHz.

carbon nanotubes (100–850 m^2g^{-1}) [37, 38]. Therefore, the overall capacitance performance of graphene nanopowder is better than the carbon nanotubes (CNTs). In other words, the capacitance of graphene-based pressure sensor is greater than the capacitance of pure CNT and CNT-composite-based pressure sensors. Therefore, for graphene sample, higher capacitance causes a smaller value of impedance (Z).

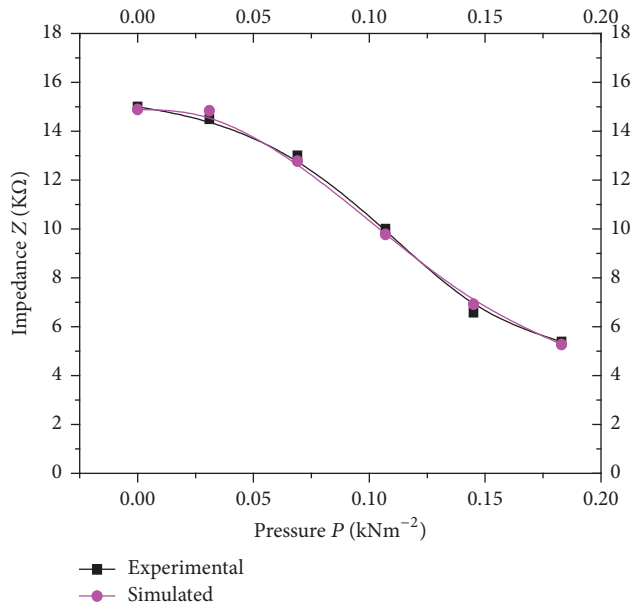

Figure 16: Impedance-pressure relationships of experimental data (Figure 14) and simulated results (11) for CNT-graphene composite-based samples at kHz.

4. Conclusion

Pure CNT, pure graphene, and CNT-graphene composite sandwich-type pressure sensors (Ag/CNT/Ag, Ag/graphene/Ag, Ag/CNT-graphene/Ag) were fabricated in the form of pellets. The sensitivities and piezoresistive properties of the samples were investigated and compared. Decrease in impedance and DC resistance with the increase in pressure was observed for all the samples. As the pressure was increased from 0 to 0.183 kNm^{-2}, the decrease percentages in DC resistance of the pure CNT, pure graphene, and CNT-graphene composite pressure sensors were 80%, 63.24%, and 70.32%, respectively. The sensitivities based on the resistance change for pure CNT, pure graphene, and CNT-graphene composite samples were 4.37, 3.44, and 3.82 m^2/kN, respectively. For the same pressure range, the decrease percentages in impedance for pure CNT, pure graphene, and CNT-graphene composite-based sample were 72.85%, 48.33%, and 64.23%, respectively. The sensitivities based on impedance decrease for pure CNT, pure graphene, and CNT-graphene composite samples were 3.98, 2.64, and 3.53 m^2/kN, respectively. The reasons for the decrease in resistance and impedance of each sample were explored. The simulated resistance-pressure and impedance-pressure relationships for the composite pressure sensor were compared with the experimental data, which exhibit an excellent agreement with each other. For all the samples, it was realized that the behavior of impedance is more dominated by the resistance effect of the pressure sensor than the corresponding capacitance effect. Moreover, the percolation theory was used to explain the conduction mechanism of the sensors. The mechanism of conductivity and the change in resistance of the sensor under the effect of pressure were also discussed.

Conflicts of Interest

The authors declare that they have no conflicts of interest.

References

[1] J. Li, *Mechanical Properties of Nanocrystalline Materials*, Pan Stanford Publishing, 2011.

[2] H.-J. Fecht, K. Brühne, and P. Gluche, *Carbon-Based Nanomaterials and Hybrids: Synthesis, Properties and Commercial Applications*, CRC Press, Boca Raton, Fla, USA, 2014.

[3] B. Marinho, M. Ghislandi, E. Tkalya, C. E. Koning, and G. De With, "Electrical conductivity of compacts of graphene, multi-wall carbon nanotubes, carbon black, and graphite powder," *Powder Technology*, vol. 221, pp. 351–358, 2012.

[4] H. Hofmann, ""Advanced nanomaterials," Powder Technology, Laboratory, 2009".

[5] J. H. Warner, F. Schaffel, M. Rummeli, and A. Bachmatiuk, *Graphene: Fundamentals and Emergent Applications*, Newnes, Australia, 2012.

[6] A. M. Hurst, S. R. Lee, N. Petrone et al., "A transconductive graphene pressure sensor," in *Proceedings of the In Sensors, Actuators and Microsystems, Transducers Eurosensors XXVII: 17th International Conference*, pp. 586–589, 2013.

[7] A. Khan, *Characterization of Organic Materials for Electromechanical Sensors*, Ghulam Ishaq Khan Institute of Engineering Sciences & Technology, Swabi, 2013.

[8] K. S. Karimov, K. Sulaiman, Z. Ahmad, K. M. Akhmedov, and A. Mateen, "Novel pressure and displacement sensors based on carbon nanotubes," *Chinese Physics B*, vol. 24, no. 1, Article ID 018801, 2015.

[9] C. M. Jureschi, J. Linares, A. Rotaru et al., "Pressure sensor via optical detection based on a 1D spin transition coordination polymer," *Sensors*, vol. 15, no. 2, pp. 2388–2398, 2015.

[10] K. S. Karimov, M. T. S. Chani, F. A. Khalid, A. Khan, and R. Khan, "Carbon nanotube - Cuprous oxide composite based pressure sensors," *Chinese Physics B*, vol. 21, no. 1, Article ID 016102, 2012.

[11] K. S. Karimov, M. Abid, M. Mahroof-Tahir et al., "V_2O_4-PEPC composite based pressure sensor," *Microelectronic Engineering*, vol. 88, no. 6, pp. 1037–1041, 2011.

[12] H. Tian, Y. Shu, X. Wang et al., "A graphene-based resistive pressure sensor with record-high sensitivity in a wide pressure range," *Scientific Reports*, vol. 5, article 8603, pp. 1–6, 2015.

[13] J. Li, W. Li, W. Huang, G. Zhang, R. Sun, and C.-P. Wong, "Fabrication of highly reinforced and compressible graphene/carbon nanotube hybrid foams via a facile self-assembly process for application as strain sensors and beyond," *Journal of Materials Chemistry C*, vol. 5, no. 10, pp. 2723–2730, 2017.

[14] P. Sahatiya and S. Badhulika, "Eraser-based eco-friendly fabrication of a skin-like large-area matrix of flexible carbon nanotube strain and pressure sensors," *Nanotechnology*, vol. 28, no. 9, Article ID 095501, 2017.

[15] J.-L. Yao, X. Yang, N. Shao, H. Luo, T. Zhang, and W.-G. Jiang, "A flexible and highly sensitive piezoresistive pressure sensor based on micropatterned films coated with carbon nanotubes," *Journal of Nanomaterials*, vol. 2016, Article ID 3024815, 5 pages, 2016.

[16] K. S. Karimov, N. Ahmed, M. M. Bashir et al., "Flexible resistive tensile load cells based on MWCNT/rubber composites," *Pigment & Resin Technology*, vol. 44, no. 3, pp. 187–191, 2015.

[17] A. Khan, K. S. Karimov, Z. Ahmad, K. Sulaiman, M. Shah, and S. A. Moiz, "Pressure sensitive organic sensor based on CNT-VO2 (3fl) Composite," *Sains Malaysiana*, vol. 43, no. 6, pp. 903–908, 2014.

[18] W. Xue and T. Cui, "Electrical and electromechanical characteristics of nano-assembled carbon nanotube thin film resistors on flexible substrates," in *Proceedings of the 4th International Conference on Solid-State Sensors, Actuators and Microsystems, (TRANSDUCERS and EUROSENSORS '07)*, pp. 1047–1050, Lyon, France, June 2007.

[19] R. J. Grow, Q. Wang, J. Cao, D. Wang, and H. Dai, "Piezoresistance of carbon nanotubes on deformable thin-film membranes," *Applied Physics Letters*, vol. 86, no. 9, Article ID 093104, pp. 93104–93107, 2005.

[20] H. Tian, Y. Yang, D. Xie et al., "Wafer-scale integration of graphene-based electronic, optoelectronic and electroacoustic devices," *Scientific Reports*, vol. 4, Article ID 03598, 9 pages, 2014.

[21] A. Lipatov, A. Varezhnikov, M. Augustin et al., "Intrinsic device-to-device variation in graphene field-effect transistors on a Si/SiO_2 substrate as a platform for discriminative gas sensing," *Applied Physics Letters*, vol. 104, no. 1, Article ID 013114, p. 13114, 2014.

[22] H.-B. Yao, J. Ge, C.-F. Wang et al., "A flexible and highly pressure-sensitive graphene-polyurethane sponge based on fractured microstructure design," *Advanced Materials*, vol. 25, no. 46, pp. 6692–6698, 2013.

[23] A. D. Smith, S. Vaziri, F. Niklaus et al., "Pressure sensors based on suspended graphene membranes," *Solid-State Electronics*, vol. 88, pp. 89–94, 2013.

[24] A. D. Smith, F. Niklaus, A. Paussa et al., "Electromechanical piezoresistive sensing in suspended graphene membranes," *Nano Letters*, vol. 13, no. 7, pp. 3237–3242, 2013.

[25] H. C. P. Movva, M. E. Ramón, C. M. Corbet et al., "Graphene field-effect transistors with self-aligned spin-on-doping of source/drain access regions," in *Proceedings of the 70th Device Research Conference, (DRC '12)*, pp. 175-176, University Park, TX, USA, June 2012.

[26] X. Chen, X. Zheng, J. K. Kim, X. Li, and D. W. Lee, "Investigation of graphene piezoresistors for use as strain gauge sensors," *Journal of Vacuum Science & Technology B*, vol. 29, no. 6, Article ID 06FE01, 2011.

[27] V. Sorkin and Y. W. Zhang, "Graphene-based pressure nanosensors," *Journal of Molecular Modeling*, vol. 17, no. 11, pp. 2825–2830, 2011.

[28] Q. Sun, D. H. Kim, S. S. Park et al., "Transparent, low-power pressure sensor matrix based on coplanar-gate graphene transistors," *Advanced Materials*, vol. 26, no. 27, pp. 4735–4740, 2014.

[29] S.-E. Zhu, M. Krishna Ghatkesar, C. Zhang, and G. C. A. M. Janssen, "Graphene based piezoresistive pressure sensor," *Applied Physics Letters*, vol. 102, no. 16, Article ID 161904, 2013.

[30] S.-H. Shin, S. Ji, S. Choi et al., "Integrated arrays of air-dielectric graphene transistors as transparent active-matrix pressure sensors for wide pressure ranges," *Nature Communications*, vol. 8, Article ID 14950, 2017.

[31] E. Mansfield, A. Feldman, A. N. Chiaramonti, J. Lehman, and A. E. Curtin, "Morphological and electrical characterization of MWCNT papers and pellets," *Journal of research of the National Institute of Standards and Technology*, vol. 120, pp. 304–315, 2015.

[32] Y. Huang, W. Wang, Z. Sun, Y. Wang, P. Liu, and C. Liu, "A multilayered flexible piezoresistive sensor for wide-ranged pressure measurement based on CNTs/CB/SR composite," *Journal of Materials Research*, vol. 30, no. 12, pp. 1869–1875, 2015.

[33] A. Ali, A. Khan, A. Ali, and M. Ahmad, "Pressure-sensitive properties of carbon nanotubes/bismuth sulfide composite materials," *Nanomaterials and Nanotechnology*, vol. 7, pp. 1–9, 2017.

[34] A. Celzard, J. F. Marêché, F. Payot, and G. Furdin, "Electrical conductivity of carbonaceous powders," *Carbon*, vol. 40, no. 15, pp. 2801–2815, 2002.

[35] A. Rani, S. Nam, K. Oh, and M. Park, "Electrical conductivity of chemically reduced graphene powders under compression," *Carbon Letters*, vol. 11, no. 2, pp. 90–95, 2010.

[36] N. Angelidis, C. Y. Wei, and P. E. Irving, "The electrical resistance response of continuous carbon fibre composite laminates to mechanical strain," *Composites Part A: Applied Science and Manufacturing*, vol. 35, no. 10, pp. 1135–1147, 2004.

[37] S. T. Saeed, *Fabrication and investigation of organic and nanomaterials based sensors [Doctoral, thesis]*, Ghulam Ishaq Khan Institute of Engineering Sciences & Technology, Swabi, 2012.

[38] W. Bauhofer and J. Z. Kovacs, "A review and analysis of electrical percolation in carbon nanotube polymer composites," *Composites Science and Technology*, vol. 69, no. 10, pp. 1486–1498, 2009.

[39] S. A. Hasan, Y. Jung, S. Kim et al., "A sensitivity enhanced MWCNT/PDMS tactile sensor using micropillars and low energy Ar+ ion beam treatment," *Sensors*, vol. 16, no. 1, p. 93, 2016.

[40] J. Shi, X. Li, H. Cheng et al., "Graphene reinforced carbon nanotube networks for wearable strain sensors," *Advanced Functional Materials*, vol. 26, no. 13, pp. 2078–2084, 2016.

[41] J. J. Niu, J. N. Wang, Y. Jiang, L. F. Su, and J. Ma, "An approach to carbon nanotubes with high surface area and large pore volume," *Microporous and Mesoporous Materials*, vol. 100, no. 1-3, pp. 1–5, 2007.

[42] Q. Ke and J. Wang, "Graphene-based materials for supercapacitor electrodes – A review," *Journal of Materiomics*, vol. 2, no. 1, pp. 37–54, 2016.

[43] R. G. Irvine, *Operational Amplifier Characteristics and Applications*, Prentice-Hall, 2ND edition, 1994.

[44] J. Fraden, *Handbook of modern sensors: physics, designs, and applications*, Springer Science & Business Media, NY, USA, 4th edition, 2010.

[45] N. Kumar, *Comprehensive Physics*, Department of Physics. S.D. G. College, Ludhian, India, 2005.

[46] M. T. S. Chani, K. S. Karimov, F. A. Khalid, and S. A. Moiz, "Polyaniline based impedance humidity sensors," *Solid State Sciences*, vol. 18, pp. 78–82, 2013.

[47] J. D. Irwin, *Basic Engineering Circuits Analysis*, John Wiley & Sons, NY, USA, 1999.